Winter 11-10-2017

Multiple Consecutive Recapture of Rigid Nanoparticles Using a Solid-State Nanopore Sensor

JungSoo Lee
Southern Methodist University, jungsool@smu.edu

MULTIPLE CONSECUTIVE RECAPTURE OF RIGID NANOPARTICLES USING A SOLID-STATE NANOPORE SENSOR

Approved by:

Dr. Min Jun Kim
Professor of Mechanical Engineering

Dr. Ali Beskok
Chair Professor of Mechanical Engineering

Dr. Jaewook Myung
Assistant Professor of Civil and Environmental Engineering

MULTIPLE CONSECUTIVE RECAPTURE OF RIGID NANOPARTICLES USING A SOLID-STATE NANOPORE SENSOR

A Dissertation Presented to the Graduate Faculty of the

Bobby B. Lyle School of Engineering

Southern Methodist University

in

Partial Fulfillment of the Requirements

for the degree of

Master of Science, Southern Methodist University

with a

Major in Mechanical Engineering

by

Jung Soo Lee

B.S., Bioengineering, Yonsei Univerisy, Seoul

May 19, 2018

ACKNOWLEDGMENTS

First and foremost I want to show my gratitude to my advisor, Dr. MinJun Kim, who gave me every resource and academic advice for my research on Master's thesis. I thank you for encouraging my research and allowing me to grow as a research scientist and engineer. Also I thank Dr. Moon Kim who gave me precious advice throughout the research in detail with the kindest heart. You gave me valuable opportunities to learn advanced imaging and nano-fabrication skills during my research.

In regard to the solid-state membrane preparation, I thank Dr. ChiWon Ahn for supporting my experiment with high quality silicon based chips and professional advice for fabricating pores.

I am grateful to BASTLAB members including Dr. Hoyeon Kim, Bin Peng, Jugal Saharia, Louis Rogowski, Sam Sheckman, Xiao Zhang with whom the research was enjoyable and manageable. Also I would like to express my thankfulness to Dr. Kevin Freedman, Dr. Gaurav Goyal, Dr. Armin Darvish who are the former nanopore team members. If it were not for your work, the research would not be here.

This work was supported by the National Institute of Health (R03EB022759), National Science Foundation (CMMI 1707818), National Research Foundation of Korea (NRF-2015K1A4A3047100, NRF-2015M3A7B6027973, NRF-2015M3A6B3068660).

Lee, Jung Soo B.S., Bioengineering, Yonsei Univerisy, Seoul

Multiple Consecutive Recapture of Rigid Nanoparticles
Using a Solid-state Nanopore Sensor

Advisor: Dr. Min Jun Kim
Master of Science, Southern Methodist University degree conferred May 19, 2018
Dissertation completed April 5, 2018

Solid-state nanopore sensors have been used to measure the size of a nanoparticle by applying a resistive pulse sensing technique. Previously, the size distribution of the population pool could be investigated utilizing data from a single translocation, however, the accuracy of the distribution is limited due to the lack of repeated data. In this study, we characterized polystyrene nanobeads utilizing single particle recapture techniques, which provide a better statistical estimate of the size distribution than that of single sampling techniques. The pulses and translocation times of two different sized nanobeads (80 nm and 125 nm in diameter) were acquired repeatedly as nanobeads were recaptured multiple times using an automated system controlled by custom-built scripts. The drift-diffusion equation was solved to find good estimates for the configuration parameters of the recapture system. The results of the experiment indicated enhancement of measurement precision and accuracy as nanobeads were recaptured multiple times. Reciprocity of the recapture and capacitive effects in solid state nanopores are discussed. Our findings suggest that solid-state nanopores and an automated recapture system can also be applied to soft nanoparticles, such as liposomes, exosomes, or viruses, to analyze their mechanical properties in single-particle resolution.

TABLE OF CONTENTS

LIST OF FIGURES

This is dedicated to the BASTLAB and its members.

Chapter 1

INTRODUCTION

1.1. Nanopore sensor platform

Nanopore-based resistive pulse sensing is a highly sensitive technique that is based on the principle that the translocation of a nanoparticle through a nanopore causes a resistive pulse in the measured electrical current. Nanopore sensors have been used to analyze various analytes such as biomacromolecules [1-6], rigid [7, 8], and deformable particles [9-11]. A constant voltage is applied at the nanopore which is locating between *Cis* and *Trans* chambers, and the constant voltage application causes a steady-state ionic current across the pore. When a nanoparticle is electrically attracted into the sensing zone around the nanopore, the

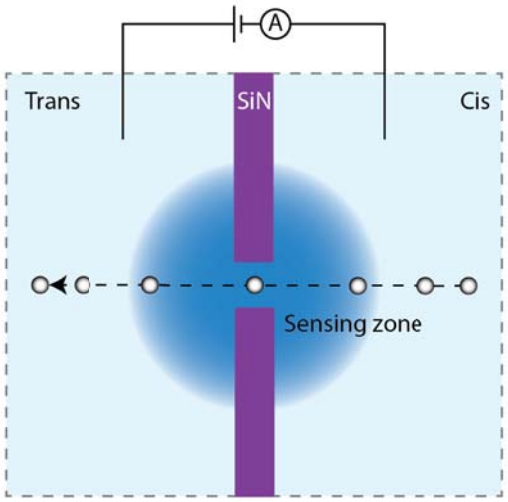

Figure 1.1. Schematic figure of nanopore sensor. The membrane separates two liquid compartments. Ions and nanoparticles move through the nanopore by electrophoresis.

resistance increases, which naturally causes a sudden current drop until the particle moves through the nanopore and escapes the sensing zone (Figure 1.1). The current is amplified

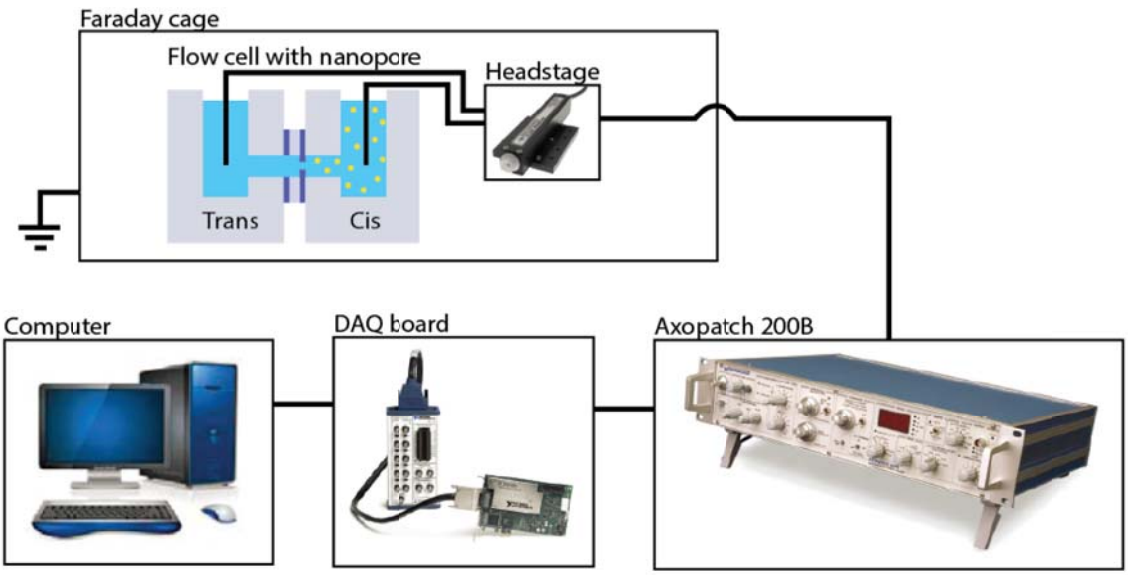

Figure 1.2. Schematic diagram of a nanopore sensor platform. The current signal is amplified and digitized by the complete nanopore platform in real time.

and digitized by amplifier (Axopatch 200B, Molecular Devices) and digitizer (BNC-2110, National Instrument) with a PCI card (Figure 1.2). Due to the electrical signal recording strategy, the signal resolution highly depends on the noise level of the system including membrane materials, solution conductivity, data collection frequency, and data frequency filtering. This technique is first introduced by Wallace H. Coulter in the late 1940s, who invented Coulter Counter which is an orifice-based resistive pulse counter for counting and sizing the red blood cells [12]. The Coulter principle is applied to develop the nanopore sensor platform to count and size any nanosized particles.

1.2. Solid-state nanopore

There are largely two types of nanopores; biological nanopores [13, 14] and solid-state nanopores [15, 16]. Biological nanopores are made of transmembrane protein channels extracted from bacteria, which can guarantee very low product variability. α-hemolysin, MspA, and Phi29 are the major biological nanopores which inner diameters of the channels are ex-

actly 1.4 nm, 1.3 nm, and 3.6 nm each. However, biological nanopore has its limitation for mass-production due to the fabrication complexity caused by channel protein installation on the lipid membrane, which requires advanced skills of hands-on training. The protein channel also has low thermal stability which causes structural deformation and functional loss depending on the surrounding temperature; data reliability for long-lasting experiment also decreases due to the low stability. Solid-state nanopores, on the other hand, are mechanically fabricated on a solid-state membrane using electron-beam or ion-beam lithography. The solid-state nanopore is superior to the biological nanopore in terms of the thermal and chemical stability, which enables long-term stable data collection for diverse particle analysis. Furthermore, the high mechanical stability allows mass production using advanced nano-manufacturing facility including e-beam or ion-beam lithography.

1.3. Single particle analysis

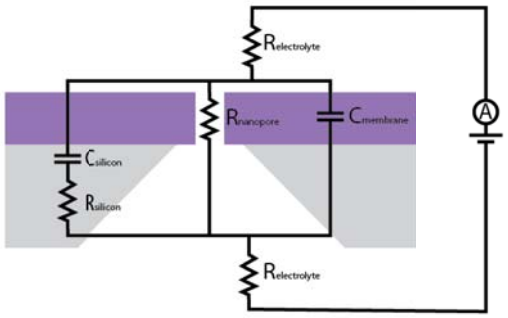

Figure 1.3. Simplified electric circuit of nanopore sensor platform. $R_{electrolyte}$ is the access resistance from the electrode to SiN membrane. $R_{silicon}$ is the resistance through the silicon substrate to the dielectric layers. $R_{nanopore}$ is the pore resistance including access resistance. $C_{membrane}$ is the capacitance of the SiN membrane. $C_{silicon}$ is the capacitance from the silicon substrate, and C_{total} would be the sum of $C_{membrane}$ and $C_{silicon}$.

While a nanoparticle enters into the sensing zone and translocates through a nanopore, resistance temporally increases and current suddenly drops until the nanoparticle escapes the sensing zone(Figure 1.3, Figure 1.4). From the extent of the current drop, the size

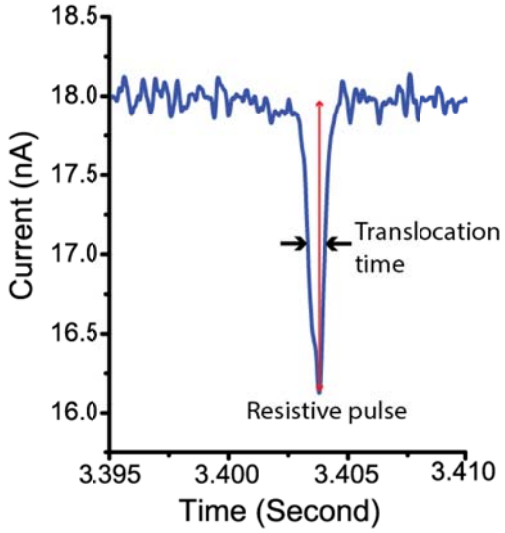

Figure 1.4. Translocation time and Peak size of a single peak; Translocation time is measured by the full width at half maximum (FWHM).

of the nanoparticle can be analytically calculated using the determined values of solution conductivity and dimensions of pore diameter and pore length. Translocation time, which is measured by the full width at half maximum (FWHM), represents the dwelling time at the sensing zone, from which the interaction between the nanoparticle and the nanopore could be analyzed. Since nanopore sensors can measure single particle properties, such as translocation time and resistive enhancement, with a single measurement, it is also possible to conduct population analysis on diluted nanoparticle suspensions [9, 10]. However, statistically, a single measurement per particle is not reliable for accurate knowledge of the size and mobility of nanoparticles. To achieve a higher level of accuracy for analyzing low concentrated nanoparticle suspensions, it is imperative that sufficient translocation data is gathered from single nanoparticle. For this purpose, recapture systems have been developed where a single particle is translocated multiple times while resistive pulse data is collected repeatedly. Until recently, nanopore recapture systems have been adopted to recapture relatively large and long DNA strands [17]. The DNA translocation induces a larger and longer resistive pulse in the baseline current than that of rigid nanoparticles; this enabled experimentalists to successfully recapture DNA more than 1000 times consecutively. Rigid

nanoparticle recaptures, however, have not been studied except the author's recent report [56].

1.4. Rigid nanoparticle

Rigid nanoparticles are good drug carriers for transdermal or cancer drug delivery, due to the faster cellular internalization when compared to soft particles [18-21]. Thus, it is crucial to measure rigid nanoparticles size and mobility accurately for the success of drug delivery applications with rigid nanoparticles. It is possible to obtain single particle information using nanopore sensors for a measurement, while other techniques to characterize single nanoparticles, such as dynamic light scattering [22] and X-ray analysis [23], provide information that depends on the ensemble measurements of nanoparticles at each measurement.

In this study, the resistive pulses and the translocation times of two different polystyrene nanobeads are analyzed. Pulse and translocation time information was collected when rigid nanoparticles translocated multiple times through the nanopore in the recapture experiments. Recapture experiments were performed to accurately measure the resistive pulse and translocation time of the two particles using in-house computer algorithms. Statistical analysis was performed to understand the refinement made by performing recapture on single particles. Lastly, several observations and limitations were reported with a nanopore sensor, based on the analysis of recaptured nanoparticles.

Chapter 2

MATERIALS AND METHODS

2.1. Nanoparticle preparation

Spherical polystyrene nanobeads of 80 nm and 125 nm were purchased (Polysciences, War-

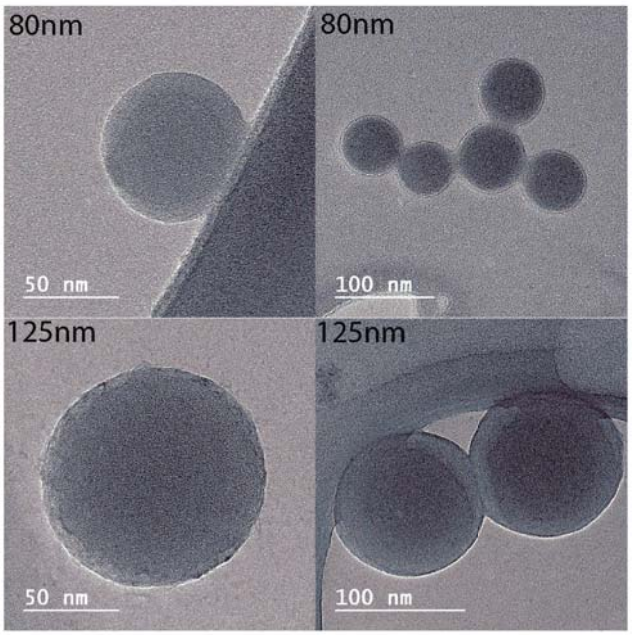

Figure 2.1. TEM pictures of 80 nm and 125 nm polystyrene nanobeads

rington, PA) and subsequently scanned with a transmission electron microscope (JEM-2100F, JEOL, Figure 2.1).

For the experiments, the particles were diluted to 10^{-5} g/ml in a buffer solution of 50 mM KCl and 20 mM phosphate buffer (pH 6). Care was exercised to keep the particle suspension colloidally stable during the translocation experiments, meaning nanoparticles were well dispersed in the buffer solution without aggregation. Chemical and mechanical methods were

used to prepare the solution. Triton X-100 was added at a concentration of 0.015 % to disperse the nanoparticles in the solution. KCl and phosphate salt concentration were controlled since high salt concentration accelerated the particle aggregation due to hydrophobic interactions [33]. The nanoparticle suspension was treated in an ultrasonic bath for 30 minutes before each experiment [34]. Dynamic light scattering experiments were employed to measure the size distribution of the particles in the buffer solution [22]. These experiments indicated no aggregation in the particle suspension (Figure 2.2).

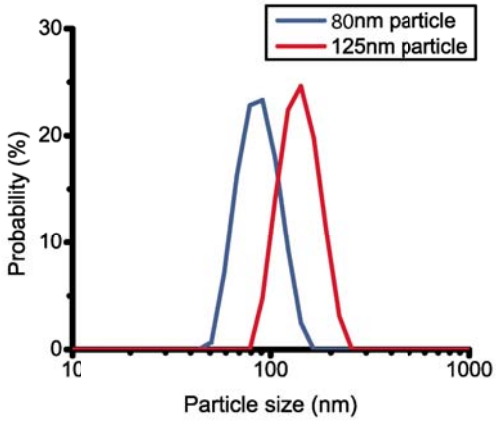

Figure 2.2. Histogram for hydrodynamic diameter of 80 nm and 125 nm polystyrene nanobeads with pH 6 Phosphate buffer solution; measurement with Zetasizer Nano ZS, Malvern

2.2. Nanopore fabrication and preparation

200 nm of a low-stressed silicon nitride (Si_xN_y) membrane was deposited on both sides of a 4-inch silicon wafer of 525 μm thickness using the low pressure chemical vapor deposition method. A 50 μm square silicon nitride window was made on the silicon wafer through microfabrication procedures of photolithography, reactive ion etching, and KOH wet etching.

Figure 2.3 shows a schematic of the etched wafer and the nanopore. A 250 nm diameter pore was fabricated using a dual-beam focused ion beam (DB-FIB, Helios Nanolab, FEI) in the 50 μm window [1, 35]. In Figure 2.4, electron microscopy micrographs of the nanopore

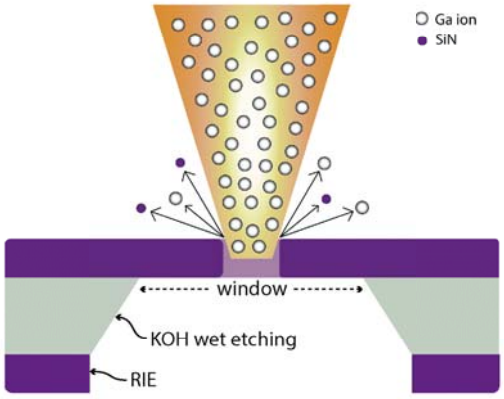

Figure 2.3. A schematic figure representing fabrication procedures of the SiN membrane and the nanopore

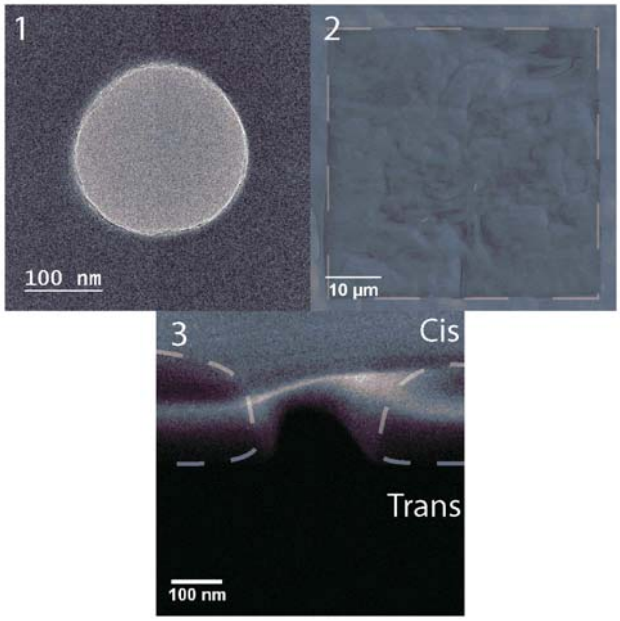

Figure 2.4. SEM and TEM pictures of nanopore 1) TEM picture of 250 nm diameter nanopore 2) SEM picture of 50 μm square SiN window 3) SEM picture of pore cross section at the pore central axis

are given. Each pore was fabricated in 7 seconds with 30 kV of acceleration voltage and 10 pA of current. Each fabricated nanopore was examined using electron micrographs, since small deformations at the nanopore edges deteriorated the quality of the translocation experiments. The third inset figure in Figure 2.4 shows the scanning electron micrographs of the nanopore cross section, where the chamfer at the rim of the nanopore is evident. The pore length (200 nm, SiN membrane thickness) was confirmed using this figure. Before the experiments, nanopore chips were cleaned using the Piranha solution for 10 minutes at 80 °C [36]. The pertinent cleaning of nanopores is important, first, to enhance the hydrophilicity of the pore for proper conductance [37-39], and second, to clean the nanopore free of debris, which could mechanically interrupt the translocation events. For the nanopore cleaning, the safety protocol suggested by the Environmental Health and Safety Department of Southern Methodist University was followed. After the cleaning, the chip was rinsed with deionized water three times.

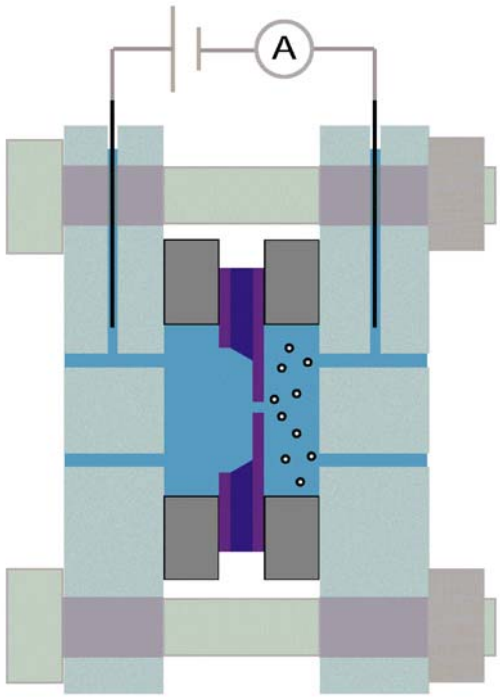

Figure 2.5. Schematic figure of the flow cell assembly

2.3. Experimental setup

The flow cell that was used to house the nanopore consists of *Cis* and *Trans* chambers. A schematic of the assembled flow cell is shown in Figure 2.5. The nanopore is positioned between the two chambers, where polydimethylsiloxane (PDMS) gaskets with an inner diameter of 3 mm separate the nanopore from the chambers. Inlet and outlet holes were drilled on the polycarbonate housing. A separate pair of inserts was used to hold a pair of Ag/AgCl electrodes. These Ag/AgCl electrodes were fabricated by soaking a 0.25 mm diameter Ag wire in bleach (Clorox) for 30 minutes. A new set of Ag/AgCl electrodes were used for every experiment, since the AgCl layer was easily worn during experiments, which could seriously exacerbate the probe sensitivity. Care was taken to avoid any bubble formation in the chambers since small bubbles could disturb or block the current. In order to facilitate the filling of the chamber, the PDMS gaskets were exposed to O_2 plasma for 3 minutes, enhancing the wetting behavior of the PDMS gasket surface. The nanoparticle suspension was introduced into the *Cis* chamber while the *Trans* chamber did not contain any nanoparticles.

2.3.1. Operation principle

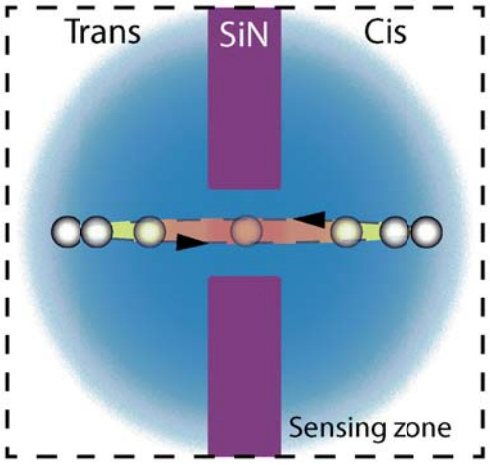

Figure 2.6. Schematic figure of nanoparticle recapture

The schematic in Figure 2.6 shows the operation principle of the experimental setup. An electric field was generated inside the chamber as the electrodes were energized at a fixed electric potential. The electric field in the flow cell was simulated using a commercial

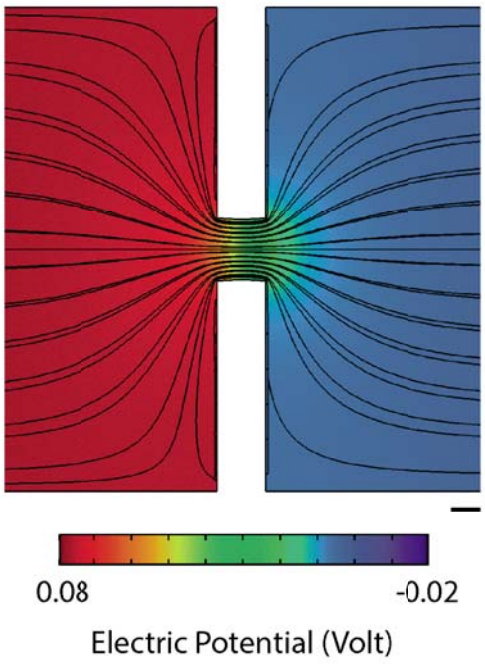

Figure 2.7. Simulation for electric field around the nanopore; Scale bar: 100 nm

solver (COMSOL Multiphysics), and given in Figure 2.7. As shown in the figure, the electric field was locally amplified in the nanopore due to the strong nanopore resistance, which caused the sudden potential drop. As a result of the interaction between the electric field and the particle charge, nanoparticles experience electrophoretic motion. Electroosmosis and dielectrophoresis are the two other mechanisms that govern particle motion. Particles could travel either to the anode or to the cathode depending on their zeta potential [40].

In Figure 2.8, the nanoparticle zeta potential, which was measured using dynamic light scattering at pH values of 6, 7, and 8, is given. The particle translocation experiments were conducted at pH 6, where the particle zeta potential was negative. The direction of particle movement in the flow cell was, therefore, from the anode to the cathode. While a nanoparticle was entering the sensing zone (Figure 2.6), the recorded current exhibited a

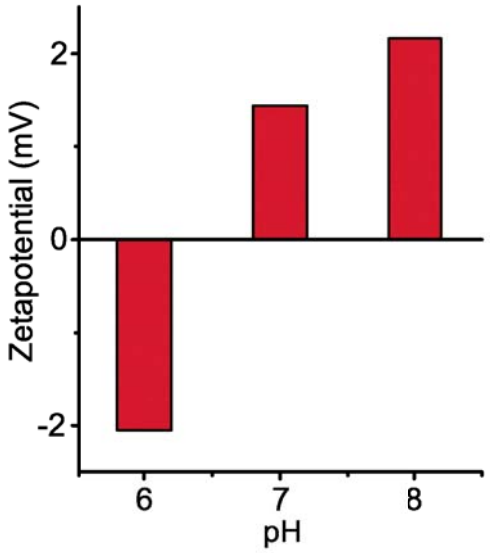

Figure 2.8. Zeta-potential measurement at different pH conditions of pH 6, 7, and 8 phosphate buffers; measurement with Zetasizer nano ZS, Malvern

sharp decrease (Figure 1.3). Analyzing this change in the measured current signal, particle properties could be inferred from signal parameters such as translocation time and peak size.

2.3.2. Data aquisition

Two electrodes connected the two electrolyte chambers to an amplifier (Axopatch 200B, Molecular Devices), which applied voltage to the electrodes and recorded the resulting current signal from the system. The current signal was processed with a digitizer (Digidata 1440A, Molecular Devices) for the pore conductance tests (Figure 2.10) or using a data acquisition board (BNC-2110, National Instrument) with a PCI card (PCI 6259, National Instrument).

The data acquisition board was used for recapture experiments since the board allowed us to modulate the polarity of the applied voltage using LabVIEW script. The current data was acquired at 30 kHz sampling frequency and filtered by a 2 kHz Bessel filter. The recorded data was analyzed using a custom-made MATLAB (MathWorks, MA) code. The function of the 2 kHz Bessel filter was to achieve a higher signal-to-noise ratio, which also facilitated

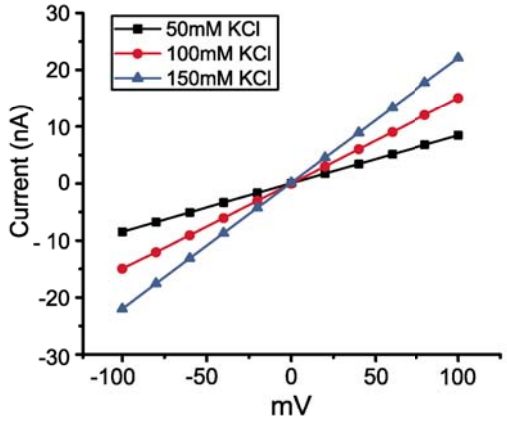

Figure 2.9. Pore conductance at different salt concentrations; KCl solutions of 50 mM, 100 mM, and 150 mM

the detection of resistive pulses in the measured signal without any loss.

2.4. Automatic feedback control recapture system

A LabVIEW (National Instruments, TX) script was developed to enable multiple recaptures of nanoparticles. The script constantly reads the current (I) from the data acquisition system and averages the recorded current at 1.67 ms windows. The script automatically changes the polarity of the applied voltage after a translocation event to achieve recapture of a particle. The following inequality is used to detect the translocation events, which is necessary for recapture.

$$I_i^k < \overline{I}_{(i-1)} - \alpha * \tau \tag{2.1}$$

In the above equation indexes i and k are for the moving average windows and the data points in the averaging windows, respectively. $\overline{I}_{(i-1)}$ is the average current at the i-1 window, τ is the peak-to-peak noise, and α is a factor, which is manually set. The script recognizes an event as a particle translocation if the current data (I_i^k) deviates more than $\alpha * \tau$ away from the previous baseline $\overline{I}_{(i-1)}$. The nanopore sensor forms an RC circuit, where the electric charge builds up at the silicon nitride layer and causes the capacitance effect (Figure 1.3, Figure 2.11).

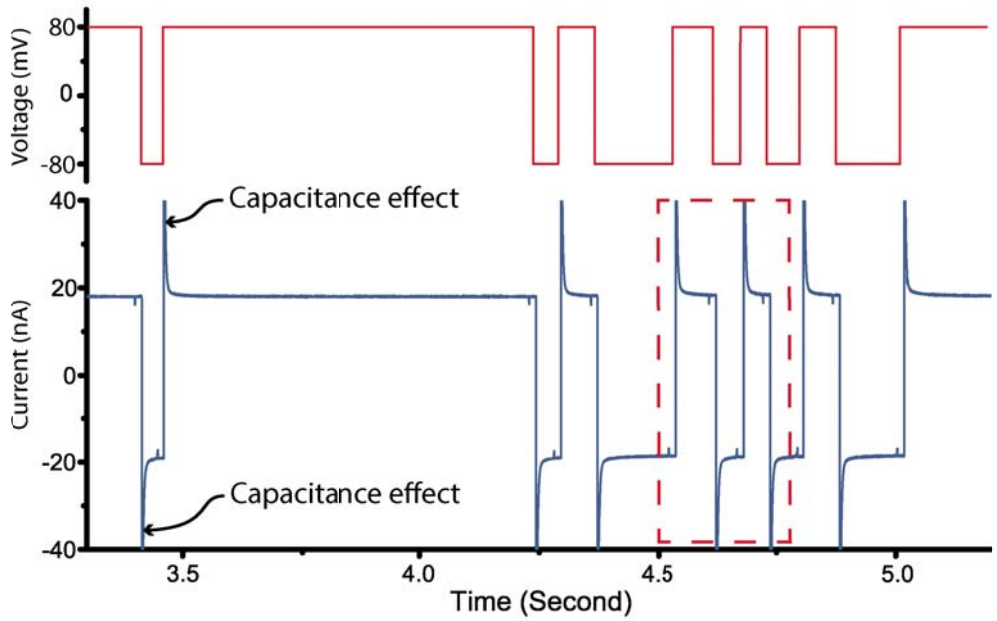

Figure 2.10. Multiple consecutive recapture events of single 125 nm nanoparticle; the above red line shows the applied voltage during the experiment.

Due to the effect, there is an exponential decrease in the current baseline, which is characterized by the settling time (T_{settle} in Figure 2.12). As the voltage polarity is reversed in the recapture experiment, the translocation event could occur during the exponential decay of the current. In this case, the detection of the translocation event becomes difficult. To avoid the recapture event to be hidden under the exponential current decay, the voltage reversal is delayed by a certain time (T_{delay} in Figure 2.12) after the detection of a translocation event, which eventually increased the recapture time ($T_{recapture}$ in Figure 2.12). This allowed the particle to avoid the exponential current decay and to be recaptured consecutively. In addition, the peak detection algorithm was disabled during the decay to prevent the script from falsely reversing the voltage polarity due to the steep current baseline (T_{skip} in Figure 2.12). Using this strategy, single particle recaptures were successfully conducted with high accuracy and reliability.

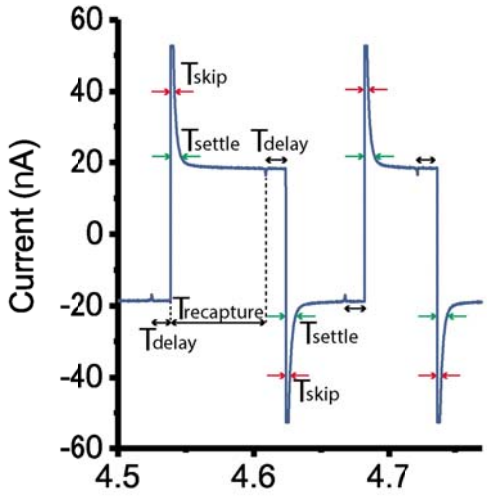

Figure 2.11. Recapture parameters for the automatic system; T_{delay} is the period between peak detection and voltage reversal. T_{skip} is the period when peak detection function of LabVIEW system is disabled to avoid the capacitance effect. T_{settle} is the period of exponential decrease of the current baseline after voltage reversal. $T_{recapture}$ is the period between voltage reversal and next peak detection.

2.5. Data analysis

For the current data with non-recaptured particles, we corrected the current baseline fluctuations by the moving average method and properly determined the peak size by iterative method, which was reported by Plesa and Dekker [41]. For the current data with recaptured particles, the identification of the translocation events was more complex, since a large number of particles got recaptured during a gradually settling current baseline (not during the beginning stage of exponential decrease) and the moving window method was no longer suitable for such scenarios. In this case, we located the translocation events using the peak detection method in the LabVIEW script and determined if the translocation event was happening on a stable current baseline. For the events on a stable current, we used the iterative method to characterize them. For the events on the settling current, we combined a third-order polynomial fitting (Figure 2.13) with the iterative method, to remove the influence of the peak on the fitting. Each time after we fit the current data, we replaced the data points which deviated more than τ (peak-to-peak noise) away from the fitting base-

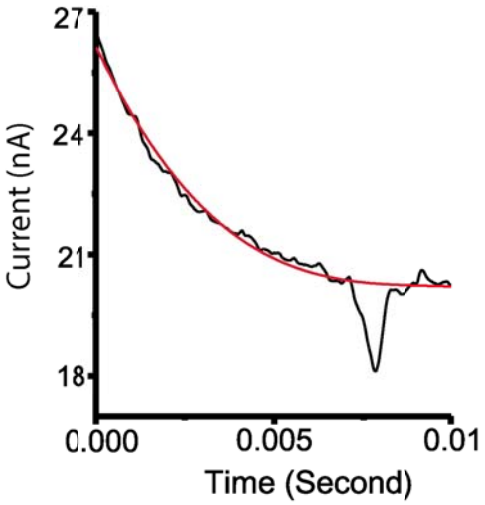

Figure 2.12. Third order polynomial fitting; the peak characterization based on the current baseline

line with the data points in the polynomial function. This fitting process lasted for three iterations, which was empirically proven to be enough to properly determine the peak size. A third-order polynomial fitting was used for the inherently exponentially settling current because only 10 ms of current data around the translocation event was investigated, which was too short for the exponential function to achieve a good fitting. The translocation time of both non-recaptured and recaptured particles was extracted using the full width at half maximum (FWHM) method [42].

2.6. Population pool analysis

The pooled mean and the pooled standard deviation formulas were applied to the experimental data. The pooled mean and the standard deviation of an ensemble measurement made on M particles are given by the following equations, respectively,

$$\overline{x} = \frac{\Sigma_{j=1}^{M} N_j \overline{x}_j}{\Sigma_{j=1}^{M} N_j} \tag{2.2}$$

$$< s_x > = \sqrt{\frac{\Sigma_{j=1}^{M} \nu_j s_{x_j}^2}{\Sigma_{j=1}^{M} \nu_j}} \tag{2.3}$$

In the above equations, x is for particle data (peak size or translocation time), $\overline{x}$ is an average performed over N_j successive recaptures, where index j is for different particles, and ν_j is the degrees of freedom.

2.7. Drift diffusion equation

The dimensionless form of the drift diffusion equation was solved to estimate a proper T_{delay} [17].

$$\frac{\delta c(r_1, s)}{\delta s} = \frac{1}{r_1^2} \frac{\delta}{\delta r_1} \mp c(r_1, s) + r_1^2 \frac{\delta c(r_1, s)}{\delta r_1} \tag{2.4}$$

where s is the dimensionless time, r_1 = r/L is a dimensionless radial coordinate, with radial distance r from the pore center and characteristic length L. The characteristic length in the above equation is the recapture distance L_c (1740.9 nm for 125 nm particles, 1044.5 nm for 80 nm particles), beyond which the electrophoretic velocity is smaller than the diffusion velocity. The negative sign is for the electrophoretic motion away from the pore, while the positive sign means the opposite. c is the volume density of the particle, which is related to the probability density function p using the following equation,

$$p = 2\pi r^2 c(r). \tag{2.5}$$

Using the above equations, we were able to compute the probability density distribution of particles at any time before and after the voltage reversal.

The following parameters were used for the solution of the drift diffusion equation with 125 nm particles: particle zeta potential, $\zeta = -2\ mV$; viscosity of the buffer solution, $\eta = 10^{-3}\ Pa * s$; electrophoretic mobility of the particle, $\mu = 1.4166 * 10^{-9}\ m^2 V^{-1} s^{-1}$; temperature, $T = 298\ K$; conductivity of the solution, $\sigma = 1.6\ S/m$; and diffusion constant of the polystyrene particles, $D = 1.6189 * 10^{-12}\ m^2 s^{-1}$; which were obtained from a previous study [43]. For brevity, the parameters and simulation results for 80 nm particles are not

shown in this thesis. The solution of the above equation was verified using benchmark data [17].

2.8. COMSOL simulation

Finite element simulation using a commercial software COMSOL Multiphysics were employed for the electric field calculations in Figure 2.7 [44]. The 2D axisymmetric computation domains (*Cis* and *Trans* chambers) were 2000 nm in diameter and 2000 nm in length, and the pore in the domain was 250 nm in diameter and 200 nm in length. Our computational model consisted of coupled Poisson, Nernst Planck, and Navier-Stokes equations enabled to simulate all the physical phenomena in the nanopore system. The locally amplified electric field was clearly illustrated by the denser electric field streamlines near the pore. 0.103 M KCl solution was used in the simulations to match the pore conductance in the experiment. An electric potential of 80 mV was applied for the simulation, which was the same voltage used for all experimental conditions. The other parameters we used for the COMSOL simulations were: diffusion constant of Potassium ion(K^+), $D_K = 1.975 * 10^{-9}\ m^2/s$; diffusion constant of Chloride ion(Cl^-), $D_{Cl} = 2.032 * 10^{-9}\ m^2/s$; membrane surface charge density, -20 mC/m^2; temperature, $T = 293.15\ K$; and viscosity of the solution, $\mu = 10^{-3}\ Pa * s$.

Chapter 3

RESULTS AND DISCUSSION

3.1. Conductance of the nanopore

Prior to the nanoparticle translocation experiments, the pore conductance tests were done to confirm the pore quality. The pore conductance was measured in the flow cell using 50 mM, 100 mM, and 150 mM KCl solutions without the nanoparticles. In these measurements, the current was measured as voltage was varied between -100 mV to 100 mV with 25 mV steps. The results are given in Figure 2.10. As the concentration of salt gets higher, the pore conductance increases allowing a larger current flow through the nanopore. The measured pore conductance using the data of the 100 mM KCl solution was 150.35 nS, which is close to the value from the analytical calculation. Assuming the pore as an empty cylinder, an analytical estimate of the conductance could be calculated using the following equation [7],

$$G = \frac{1}{R_{pore} + R_{acc}} = \frac{\pi \sigma D^2}{4L + \pi D} \tag{3.1}$$

where D and L are pore diameter and pore length, σ is the conductivity of the solution, R_{pore} and R_{acc} are the geometrical resistance and access resistance of the pore, respectively. Since the pore length (200 nm) and diameter (250 nm) have similar values, the access resistance contributes to nearly half of the overall resistance. The experimentally measured value of the pore conductance is 5.16 % lower than the theoretical value of 158.53 nS. This small difference between experimental and theoretical results could be due to the asymmetric geometry of the nanopore, and to the resistive effects of the electrode polarization.

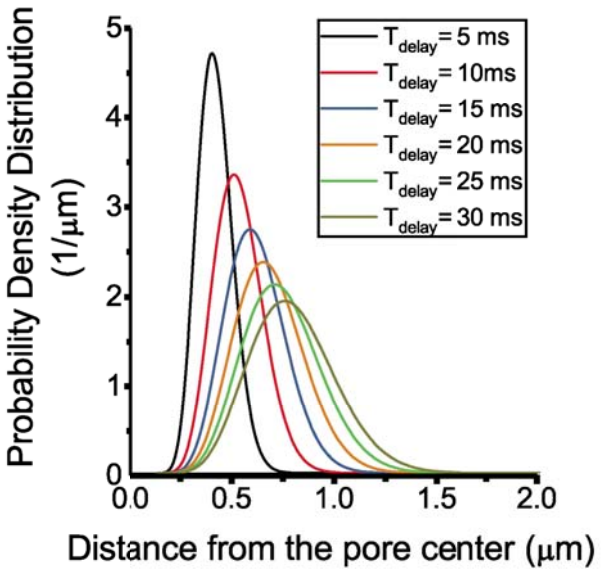

Figure 3.1. Simulation for Probabillity density distribution with different T_{delay} for 125nm nanoparticles

3.2. Recapture probability

Recapture kinetics were studied by computer simulation. In Figure 3.1, the probability density distribution of 125 nm polystyrene nanobeads is shown for different delaying times. The location of the peak in the probability density function moves away from the pore center due to the electrophoretic force as a function of the delaying time. To find the recapture probability after the voltage reversal with a certain delay time, the area under the probability density curve is integrated from the origin to a distance of 250 nm, which is the diameter of the particle plus the half length of the pore. It is assumed that the particles could be recaptured by 100 % chance within 250 nm radial distance from the pore center. Figure 3.2 shows that the highest recapture probability for 125 nm particles drastically drops from 8.60 % to 0.71 %, while the delaying time increases from 5 ms to 30 ms. Such estimation of recapture probability offered a theoretical background to properly choose the key parameters for the recapture experiment. For example, we chose the delaying time between 5 ms and 20 ms in the experiment, since further increase in delaying time would result in extremely

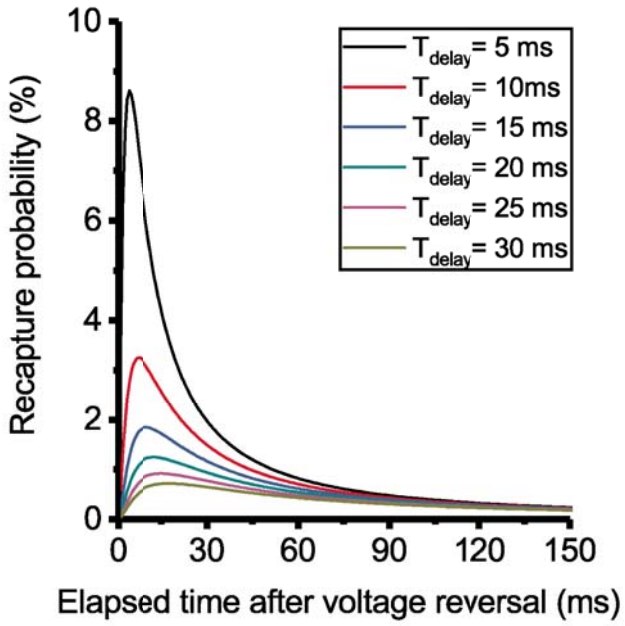

Figure 3.2. Simulation for Recapture probability with different T_{delay} for 125 nm nanoparticles.

low recapture probability.

3.3. Recapture experiment

We succeeded at consecutive multiple recaptures of single particles during the recapture experiments. Representative traces of the recorded current of 80 nm and 125 nm single particles were shown in Figure 2.11 and Figure 3.3. In these figures, as a translocation was identified by the system, the voltage polarity was automatically reversed after a certain delay time. The current baseline after the settling time in Figure 3.3(c) was about 21 pA, which was higher than the current baseline of Figure 3.3(a) and Figure 3.3(b). This was because a higher phosphate buffer concentration was used for the 80 nm particle recapture experiment in Figure 3.3(c). Recapture data from nine individual 125 nm particles is given in Figure 3.4, where the average current drop is plotted for each particle with its standard deviation. The small standard deviation of each set demonstrated that we consecutively captured the same particles. To be specific, the averaged standard deviation value was 0.129, which was

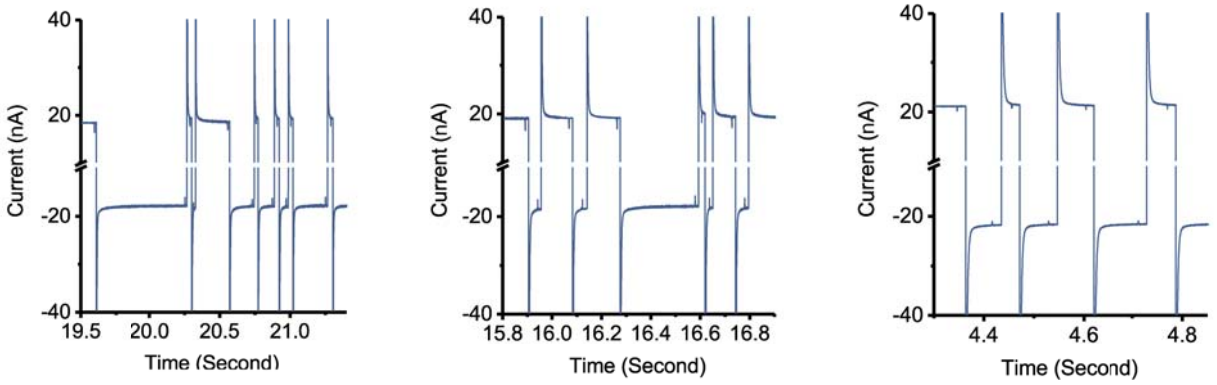

Figure 3.3. Single particle recapture data (a) Recapture data with 125nm bead. T_{delay}: 12.5 ms, T_{skip}: 12 ms, 15 mM pH 6 phosphate buffer with 50 mM (b) Recapture experiment data with 125 nm bead. T_{delay}: 12.5 ms, T_{skip}: 12 ms, 15 mM pH 6 phosphate buffer with 50 mM KCl (same experimental condition with figure 3.3(a)) (c) Recapture experiment data with 80 nm bead. T_{delay}: 15 ms, T_{skip}: 15ms, 20 mM pH 6 phosphate buffer 50 mM KCl

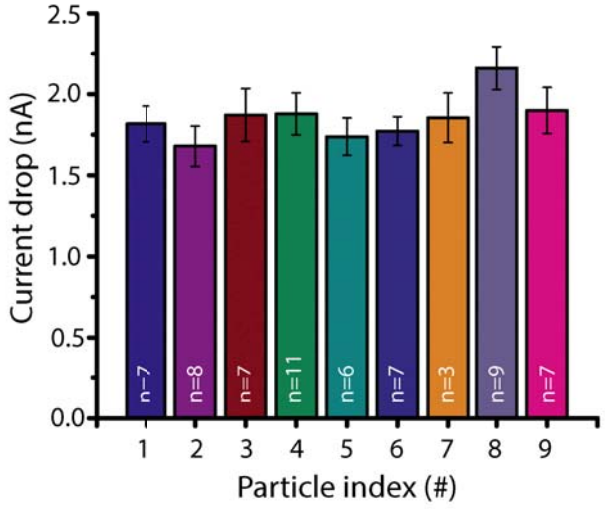

Figure 3.4. Bar chart for single particle analysis by comparing nine sets of recapture events from nine nanoparticles

about one third of the standard deviation 0.383 of the population pool.

After testing its feasibility for single particle analysis, the peak size and translocation time distributions of single translocation and recapture data were calculated. The comparison of translocation time and peak size distribution is given in Figure 5 for 80 nm and 125 nm particles. Figure 3.5 show the peak size and translocation time for 80 nm and 125 nm particles. Shown in the figure is the pooled mean and its standard deviation that are weighted by the recapture times. Results for 80 nm particles in Figure 3.4 indicated that there was a significant decrease of standard deviation in the recapture data (peak size and translocation time) when compared to the single translocation data. Accordingly, multiple recaptures increased the precision of the measurement made by the nanopore system for 80 nm particles. For 125 nm particles, on the other hand, no such significant reduction was evident in the peak size and translocation time data. The possible explanation for the size dependency is discussed on the section 3.4 and 3.5. Assuming the pore is of cylindrical shape, the relative excluded volume (χ, defined as the relative volume excluded by the particle in the pore) is [7]

$$\chi = \frac{2D_{particle}^3}{3L_{pore}D_{pore}^2}, \tag{3.2}$$

which is valid only when $D_{particle} \leq L_{pore}$. It can be deduced that the current blockade is proportional to the cube of the particle diameter $\Delta I \sim \chi \sim D_{particle}^3$. Therefore, according to the above equation, the ratio of the peak sizes for 80 nm and 125 nm particles is 3.8147. Experimentally, the peak size ratio for recapture and single translocation data is 3.9384 and 4.2427, respectively. The data with recaptured particles thus provided a closer match to the estimate for the peak size ratio predicted by equation 3.2. The refinement of the nanopore measurements with recapture, therefore, not only increased precision of the measurement but also exhibited a closer match with the theory.

3.4. Size dependency of the recapture event

There are a few possible reasons to explain the size dependency of the recapture data. The

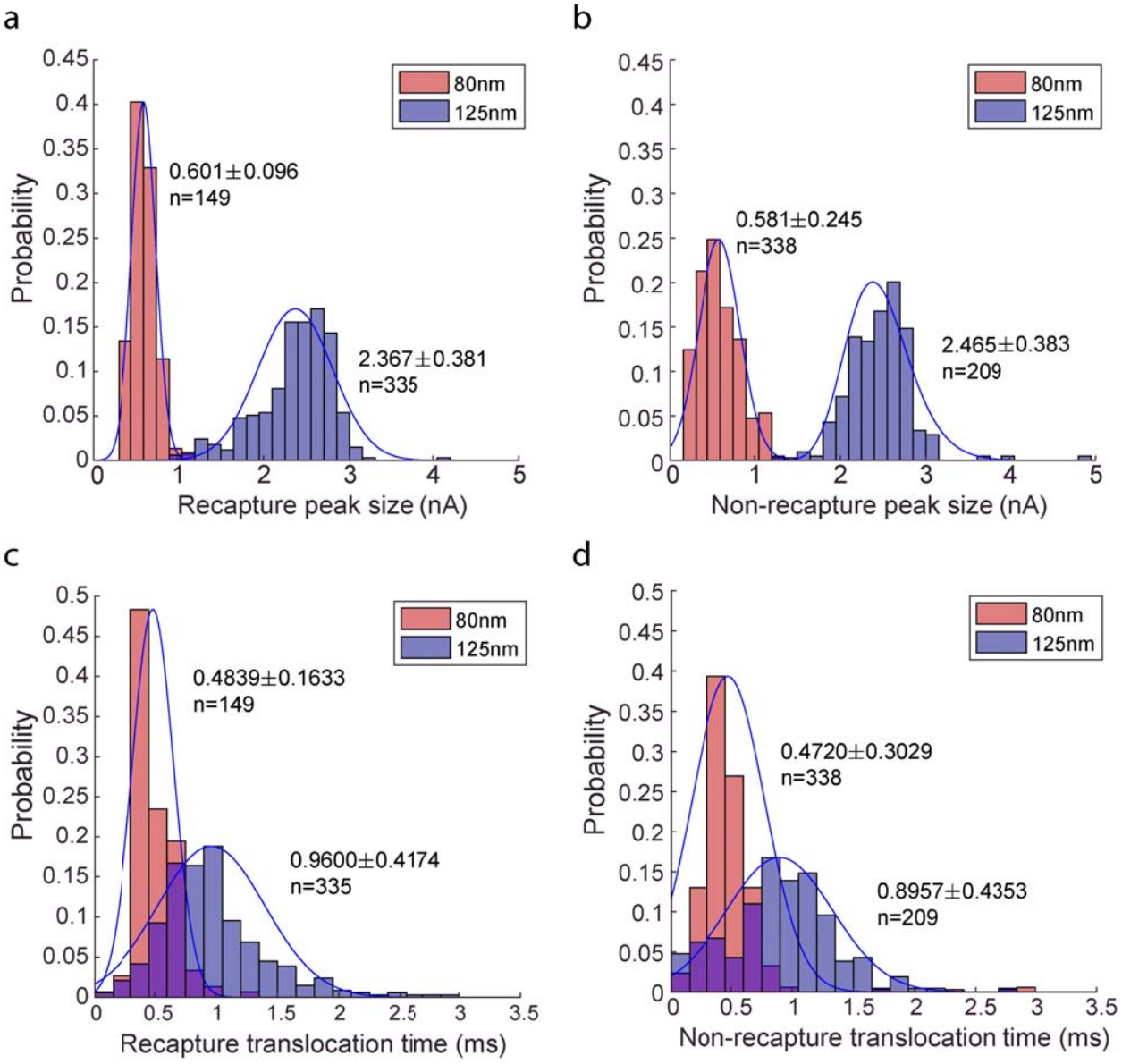

Figure 3.5. Comparison between recapture and single translocation data (a) Histogram of peak sizes of 80 nm and 125 nm nanoparticles using the recapture data (b) Histogram of peak sizes of 80 nm and 125 nm nanoparticles using the single translocation data (c) Histogram of translocation times of 80 nm and 125 nm nanoparticles using the recapture data (d) Histogram of translocation times of 80 nm and 125 nm nanoparticles using the single translocation data

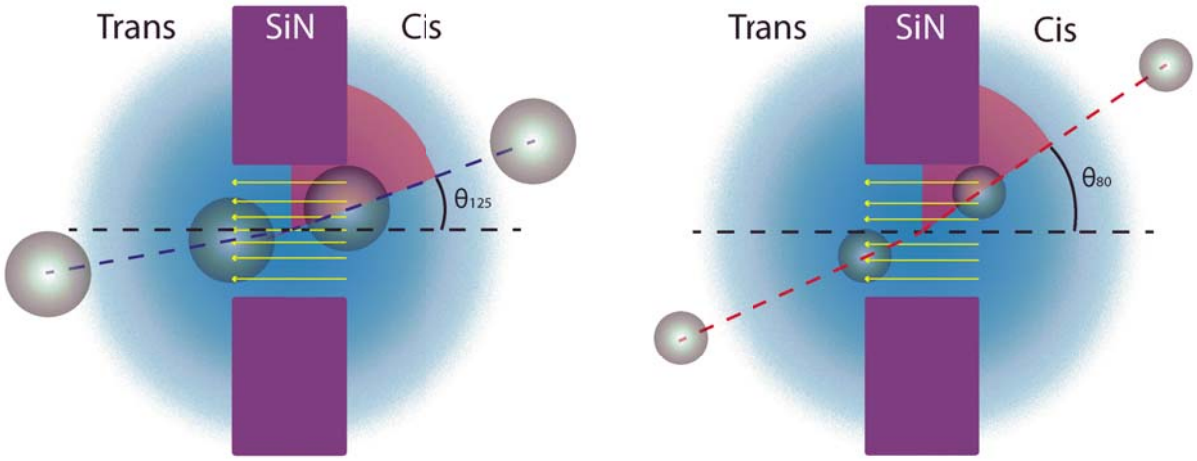

Figure 3.6. The access angle effect depending on translocation direction (a) A schematic figure for the access angle effect of 125 nm nanoparticle (b) A schematic figure for the access angle effect of 80 nm nanoparticle

access angle effect is the first one, which affects the translocation time depending on the particle and pore size. Figure 3.6 show that the 125 nm diameter particle has a smaller maximum access angle (Θ_{125}), which is defined by the intersection angle between the trajectory and the pore axis, than that of the 80 nm particle (Θ_{80}). If the particle is out of the maximum access angle, it has a higher chance to collide with the wall of the pore and change its trajectory inside the pore, which eventually makes the particle stay longer inside the pore and increases the translocation time. The access angle of the 80 nm (Θ_{80}, 88 nm at the distribution peak) and the 125 nm (Θ_{125}, 140 nm at the distribution peak) are 39° and 28.8° respectively. The area out of the access angle zone ($90° - \theta$, red area of Figure 3.6) can be regarded as the area from which the particle moves toward the pore and collides with the wall. If we hypothesize that the particles around the pore have the same chances to access the pore, 125 nm particles have a 68 % ($61.2°/90° * 100\%$) probability to collide with the wall of the pore, which is 11.3 % higher than that of 80 nm particles. This access angle effect eventually makes it much more likely for the 125 nm particle to collide with the wall of the nanopore and spend more time within it during the translocation. On top of that, the

number of collisions of the translocating particle is increased by the asymmetric geometry of the nanopore, which will be further discussed in section 3.5.

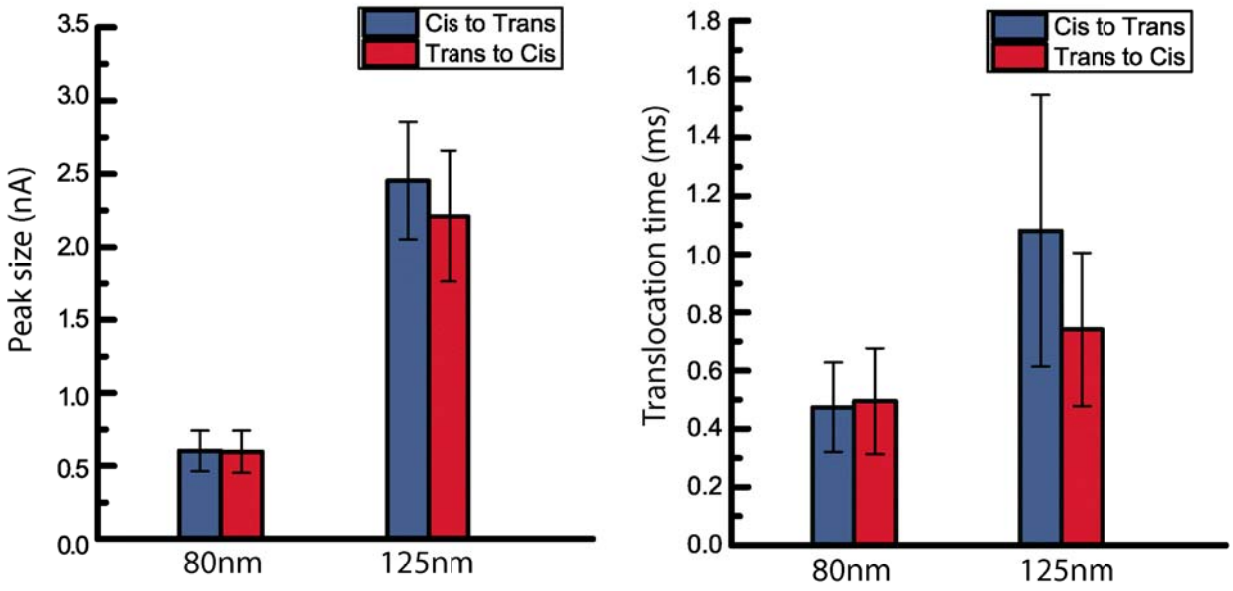

Figure 3.7. Peak size and translocation time depending on translocation direction (a) Bar chart for peak sizes of *Cis to Trans* and *Trans to Cis* translocation events (b) Bar chart for translocation times of *Cis to Trans* and *Trans to Cis* translocation events

3.5. Reciprocity of the recapture event

The recapture and non-recapture (single translocation) events from 80 nm and 125 nm polystyrene nanobeads were recorded, and the data population was divided into two sub-populations that were based on the direction of the translocation, namely *Cis to Trans* and *Trans to Cis*. Using statistical analysis, *Cis to Trans* events and *Trans to Cis* events were compared with regards to peak size (Figure 3.7(a)) and translocation time (Figure 3.7(b)). In case of 80 nm particles, there was no significant difference between *Cis to Trans* and *Trans to Cis* in peak size and translocation time. For 125 nm particles, however, a significant difference was observed in translocation time, where *Cis to Trans* translocation took about one-half longer than *Trans to Cis* on average. To further prove the observation, the Welchs

test [52] was performed. The t value was 5.9770, which was sufficient to show the statistical significance at a level of 0.05. A possible explanation for the translocation time imbalance is

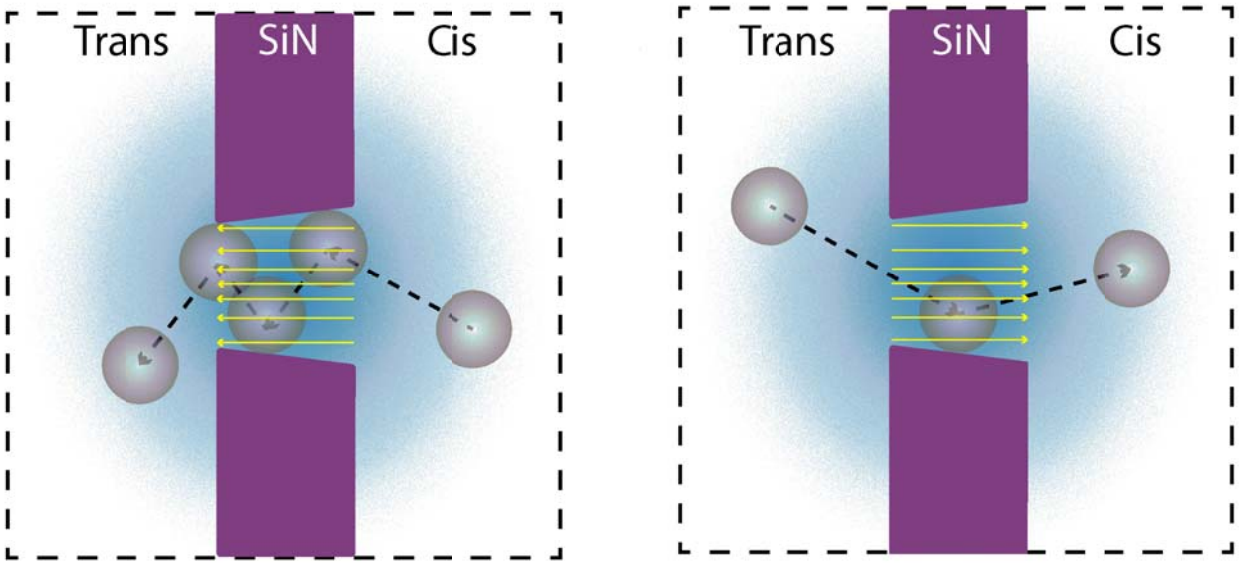

Figure 3.8. Asymmetric pore structure and translocation direction (a) Schematic figure of the asymmetric pore geometry for the *Cis to Trans* translocation (b) Schematic figure of the asymmetric pore geometry for the *Trans to Cis* translocation

that the asymmetrical pore geometry makes the translocation time different according to the direction. The pore geometry is not completely cylindrical across the pore axis, and could be regarded as a truncated cone shape (Figure 2.4(3)), the bottom surface of which becomes a *Cis to Trans* translocation entrance. Since the entrance of *Cis to Trans* translocation has a larger area than that of *Trans to Cis*, the particle enters the pore easily, but becomes harder to get out (Figure 3.8(a)). On the contrary, in the case of *Trans to Cis* translocation, it becomes harder for the particle to enter the pore, but easier to escape (Figure 3.8(b)). The asymmetrical pore geometry affects the translocation time of 125 nm particles more than that of 80 nm particles because the size of the translocating particle is proportional to the chance of the particle to collide with the wall. Therefore, we assume that the access angle and pore geometry both affect the translocation time of the particle depending on its size and direction.

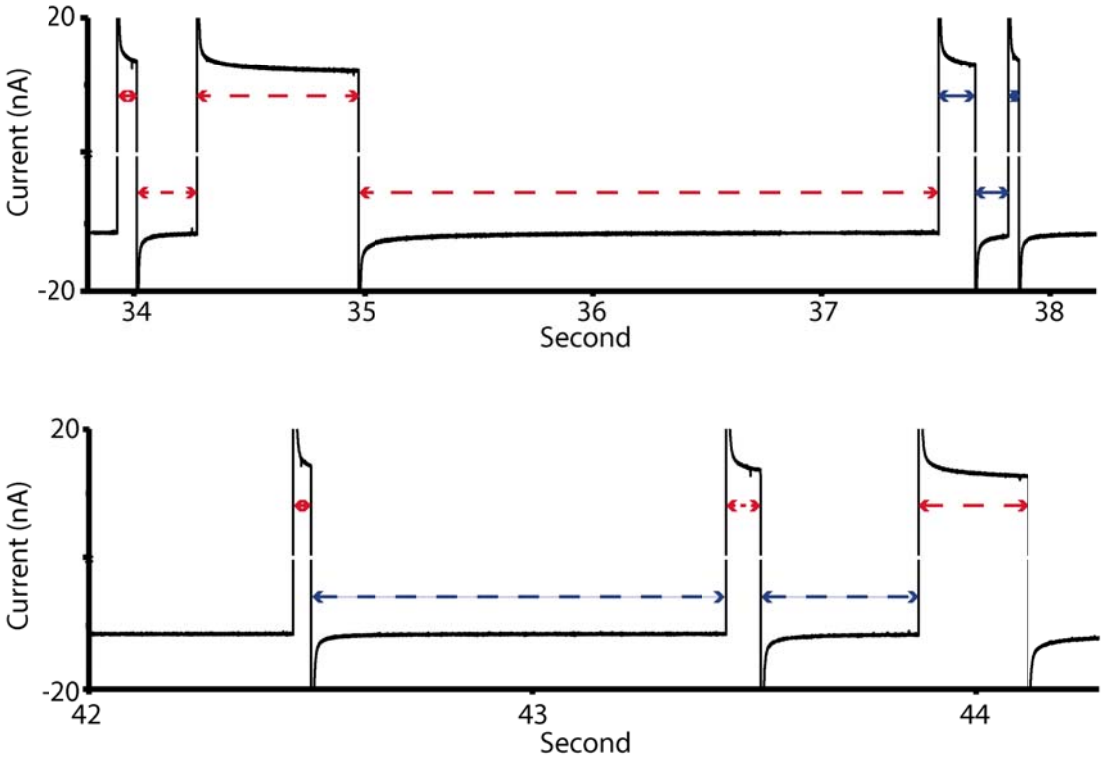

Figure 3.9. Particl recapture dynamics (a) Current trace in a recapture experiment of 125 nm polystyrene nanoparticle. Recapture zone increased and then decreased both in *Cis* and *Trans* chambers (b) Current trace in a recapture experiment of 125 nm polystyrene nanoparticle. Recapture zone increased in *cis* chamber, but decreased in *Trans* chamber.

3.6. Particle recapture dynamics

As we repeatedly conducted the recapture experiments, we observed several interesting patterns in the dynamics of nanoparticle recapture. We can infer the recapture dynamics from the recapture time which represents the recapture zone to which the particle moves and returns in both chambers. Two representative current traces are given in Figures 3.9. The recapture time in Figure 3.9(a) increased for the first 37.5 seconds of the experiment and decreased after 37.5 seconds. In other words, the recapture zone increased and then decreased both in *Cis* and *Trans* chambers. In Figure 3.9(b), the recapture time of *Cis to Trans* events and *Trans to Cis* changed in an opposite way. The recapture time of *Cis to Trans* got longer, but the recapture time of *Trans to Cis* got shorter as more recapture events happened. The recapture zone in *Cis* chamber increased, but decreased in *Trans* chamber.

3.7. Challenges and solutions

In any case, the recaptured particles got lost after a few recaptures. Since 20 ms of delay time was applied, there was a low possibility of the particle diffusing away from the nanopore. We, therefore, assume that most of the lost peaks appeared on the exponential decay right after the voltage reversal. There are two solutions to overcome this challenge. The first solution is to reduce the settling time by material engineering. Silicon dioxide (SiO_2), for example, is a good material with low capacitance effect [53, 54]. The second solution is to increase the delay time which postpones the recapture of the particle by an automatic delay time control algorithm. If the delay time increases, the recapture time will also increase, and vice versa.

Chapter 4

CONCLUDING REMARKS

Nanoparticle characterization is a crucial step in developing better drug delivery systems for treating cancers and genetic diseases. We built an automatic single-particle recapture system for rigid nanoparticles by combining solid-state nanopores and resistive pulse sensing techniques. We demonstrated the feasibility of this platform for analysis of single nanoparticles with high accuracy and reliability by performing pooled data analysis on the recapture and non-recapture events [56]; this shows its potential to be applied for early diagnosis by detection of therapeutic targets of low concentration in the bloodstream.

There are still a few challenges that need to be overcome for a limitless single nanoparticle recapturing system. This nanopore recapture platform is, however, opening new possibilities for single-particle analysis strategy from micro-size to nano-size rigid and soft particles. This technique, in particular, could be applied on soft nanoparticles, such as liposomes, exosomes, or viruses to measure their mechanical properties such as rigidity and area-expansion modulus [10], which could eventually answer varied biological and pathological phenomena of budding and fusion in cellular biology.

Chapter 5

REFERENCES

[1] Kim, M.J., et al., Rapid Fabrication of Uniformly Sized Nanopores and Nanopore Arrays for Parallel DNA Analysis. Advanced Materials, 2006. 18(23): p. 3149-3153.

[2] Freedman, K.J., C.W. Ahn, and M.J. Kim, Detection of Long and Short DNA Using Nanopores with Graphitic Polyhedral Edges. ACS Nano, 2013. 7(6): p. 5008-5016.

[3] Freedman, K.J., et al., Chemical, Thermal, and Electric Field Induced Unfolding of Single Protein Molecules Studied Using Nanopores. Anal. Chem., 2011. 83(13): p. 5137-5144.

[4] Freedman, K.J., et al. Single molecule protein biophysics using chemically modified nanopores. in 2010 IEEE Sensors. 2010.

[5] Goyal, G., et al., Hydrophilic and size-controlled graphene nanopores for protein detection. Nanotechnology, 2016. 27(49): p. 495301.

[6] Larkin, J., et al., High-Bandwidth Protein Analysis Using Solid-State Nanopores. Biophys. J., 2014. 106(3): p. 696-704.

[7] Goyal, G., et al., Low aspect ratio micropores for singleparticle and singlecell analysis. Electrophoresis, 2015. 36(9-10): p. 1164-1171.

[8] Goyal, G., K.J. Freedman, and M.J. Kim, Gold Nanoparticle Translocation Dynamics and Electrical Detection of Single Particle Diffusion Using Solid-State Nanopores. Anal. Chem., 2013. 85(17): p. 8180-8187.

[9] Darvish, A., et al., Nanoparticle mechanics: deformation detection via nanopore resistive pulse sensing. Nanoscale, 2016. 8(30): p. 14420-14431.

[10] Goyal, G., A. Darvish, and M.J. Kim, Use of solid-state nanopores for sensing co-translocational deformation of nano-liposomes. Analyst, 2015. 140(14): p. 4865-4873.

[11] Wster, P., et al., Extracellular vesicles are transferred from melanocytes to keratinocytes after UVA irradiation. Sci. Rep., 2016. 6: p. 27890.

[12] Robinson, J.P., Wallace H. Coulter: Decades of invention and discovery. Cytometry Part A, 2013. 83(5): p. 424-438.

[13] Rafael, M., et al., Nanopore-Based Devices for Bioanalytical Applications. JALA: Journal of the Association for Laboratory Automation, 2010. 15(3): p. 243-252.

[14] Butler, T.Z., J.H. Gundlach, and M. Troll, Ionic Current Blockades from DNA and RNA Molecules in the -Hemolysin Nanopore. Biophysical Journal, 2007. 93(9): p. 3229-3240.

[15] Freedman, K.J., et al., Solid-State Nanopore Detection of Protein Complexes: Applications in Healthcare and Protein Kinetics. Small, 2013. 9(5): p. 750-759.

[16] Goyal, G., K.J. Freedman, and M.J. Kim, Gold Nanoparticle Translocation Dynamics and Electrical Detection of Single Particle Diffusion Using Solid-State Nanopores. Analytical Chemistry, 2013. 85(17): p. 8180-8187.

[17] Gershow, M. and J.A. Golovchenko, Recapturing and trapping single molecules with a solid-state nanopore. Nature nanotechnology, 2007. 2(12): p. 775-779.

[18] Geng, Y., et al., Shape effects of filaments versus spherical particles in flow and drug delivery. Nature nanotechnology, 2007. 2(4): p. 249-255.

[19] Sun, J., et al., Tunable rigidity of (polymeric core)(lipid shell) nanoparticles for regulated cellular uptake. Advanced Materials, 2015. 27(8): p. 1402-1407.

[20] Anselmo, A.C. and S. Mitragotri, Impact of particle elasticity on particle-based drug delivery systems. Advanced drug delivery reviews, 2017. 108: p. 51-67.

[21] Ramezanpour, M., et al., Computational and experimental approaches for investigating nanoparticle-based drug delivery systems. Biochimica et Biophysica Acta (BBA)-Biomembranes, 2016. 1858(7): p. 1688-1709.

[22] Pecora, R., Dynamic light scattering measurement of nanometer particles in liquids. Journal of nanoparticle research, 2000. 2(2): p. 123-131.

[23] Khorsand Zak, A., et al., X-ray analysis of ZnO nanoparticles by WilliamsonHall and sizestrain plot methods. Solid State Sciences, 2011. 13(1): p. 251-256.

[24] Kim, M.J., et al., Rapid Fabrication of Uniformly Sized Nanopores and Nanopore Arrays for Parallel DNA Analysis. Adv. Mater., 2006. 18(23): p. 3149-3153.

[25] Geng, Y., et al., Shape effects of filaments versus spherical particles in flow and drug delivery. Nat. Nanotechnol., 2007. 2(4): p. 249-255.

[26] Sun, J., et al., Tunable rigidity of (polymeric core)(lipid shell) nanoparticles for regulated cellular uptake. Adv. Mater., 2015. 27(8): p. 1402-1407.

[27] Anselmo, A.C. and S. Mitragotri, Impact of particle elasticity on particle-based drug delivery systems. Adv. Drug Delivery Rev., 2017. 108: p. 51-67.

[28] Ramezanpour, M., et al., Computational and experimental approaches for investigating nanoparticle-based drug delivery systems. Biochim. Biophys. Acta, Biomembr., 2016. 1858(7): p. 1688-1709.

[29] Pecora, R., Dynamic light scattering measurement of nanometer particles in liquids. J. Nanopart. Res., 2000. 2(2): p. 123-131.

[30] Zak, A.K., et al., X-ray analysis of ZnO nanoparticles by WilliamsonHall and sizestrain plot methods. Solid State Sciences, 2011. 13(1): p. 251-256.

[31] Gershow, M. and J.A. Golovchenko, Recapturing and trapping single molecules with a solid-state nanopore. Nat. Nanotechnol., 2007. 2(12): p. 775-779.

[32] Plesa, C., et al., Non-equilibrium folding of individual DNA molecules recaptured up to 1000 times in a solid state nanopore. Nanotechnology, 2013. 24(47): p. 475101.

[33] Jiang, X., Hydrophobic-lipophilic interactions. Aggregation and self-coiling of organic molecules. Accounts of Chemical Research, 1988. 21(10): p. 362-367.

[34] Zhao, J., S. Pispas, and G. Zhang, Effect of Sonication on Polymeric Aggregates Formed by Poly (ethylene oxide)Based Amphiphilic Block Copolymers. Macromolecular Chemistry and Physics, 2009. 210(12): p. 1026-1032.

[35] Miles, B.N., et al., Single molecule sensing with solid-state nanopores: novel materials, methods, and applications. Chemical Society Reviews, 2013. 42(1): p. 15-28.

[36] Wanunu, M. and A. Meller, Chemically modified solid-state nanopores. Nano letters, 2007. 7(6): p. 1580-1585.

[37] Kowalczyk, S.W., et al., Modeling the conductance and DNA blockade of solid-state nanopores. Nanotechnology, 2011. 22(31): p. 315101.

[38] Smeets, R.M., et al., Salt dependence of ion transport and DNA translocation through solid-state nanopores. Nano Lett, 2006. 6(1): p. 89-95.

[39] Cervera, J., B. Schiedt, and P. Ramirez, A Poisson/Nernst-Planck model for ionic transport through synthetic conical nanopores. EPL (Europhysics Letters), 2005. 71(1): p. 35.

[40] Schuetzner, W. and E. Kenndler, Electrophoresis in synthetic organic polymer capillaries: variation of electroosmotic velocity and. zeta. potential with pH and solvent composition. Analytical Chemistry, 1992. 64(17): p. 1991-1995.

[41] Plesa, C. and C. Dekker, Data analysis methods for solid-state nanopores. Nanotechnology, 2015. 26(8): p. 084003.

[42] Pedone, D., M. Firnkes, and U. Rant, Data analysis of translocation events in nanopore experiments. Analytical chemistry, 2009. 81(23): p. 9689-9694.

[43] Dunstan, D.E. and J. Stokes, Diffusing Probe Measurements of Polystyrene Latex Particles in Polyelectrolyte Solutions: Deviations from Stokes Einstein Behavior. Macromolecules, 2000. 33(1): p. 193-198.

[44] Liu, S., T.D. Yuzvinsky, and H. Schmidt, Effect of fabrication-dependent shape and composition of solid-state nanopores on single nanoparticle detection. ACS nano, 2013. 7(6): p. 5621-5627.

[45] Jiang, X., Hydrophobic-lipophilic interactions. Aggregation and self-coiling of organic molecules. Acc. Chem. Res., 1988. 21(10): p. 362-367.

[46] Zhao, J., S. Pispas, and G. Zhang, Effect of Sonication on Polymeric Aggregates Formed by Poly (ethylene oxide)Based Amphiphilic Block Copolymers. Macromol. Chem. Phys., 2009. 210(12): p. 1026-1032.

[47] Wanunu, M. and A. Meller, Chemically modified solid-state nanopores. Nano Lett., 2007. 7(6): p. 1580-1585.

[48] Smeets, R.M., et al., Salt dependence of ion transport and DNA translocation through solid-state nanopores. Nano Lett., 2006. 6(1): p. 89-95.

[49] Cervera, J., B. Schiedt, and P. Ramirez, A Poisson/Nernst-Planck model for ionic transport through synthetic conical nanopores. Europhys. Lett., 2005. 71(1): p. 35.

[50] Schuetzner, W. and E. Kenndler, Electrophoresis in synthetic organic polymer capillaries: variation of electroosmotic velocity and. zeta. potential with pH and solvent composition. Anal. Chem., 1992. 64(17): p. 1991-1995.

[51] Pedone, D., M. Firnkes, and U. Rant, Data analysis of translocation events in nanopore experiments. Anal. Chem., 2009. 81(23): p. 9689-9694.

[52] Welch, B.L., The significance of the difference between two means when the population variances are unequal. Biometrika, 1938. 29(3/4): p. 350-362.

[53] Janssen, X.J., et al., Rapid manufacturing of low-noise membranes for nanopore sensors by trans-chip illumination lithography. Nanotechnology, 2012. 23(47): p. 475302.

[54] Rosenstein, J.K., et al., Integrated nanopore sensing platform with sub-microsecond temporal resolution. Nature methods, 2012. 9(5): p. 487-492.

[55] Rosenstein, J.K., et al., Integrated nanopore sensing platform with sub-microsecond temporal resolution. Nat. Methods, 2012. 9(5): p. 487-492.

[56] Lee, J.S., B. Peng, A.C. Sabuncu, S. Nam, C. Ahn, Moon J. Kim, MinJun Kim, Multiple consecutive recapture of rigid nanoparticles using a solid-state nanopore sensor. Electrophoresis, 2018, 39(5-6): p. 833-843.

Appendix A

PAPER AND POSTER

Journal Paper

J.S. Lee, B. Peng, A.C. Sabuncu, S. Nam, C. Ahn, Moon J. Kim, MinJun Kim

Multiple consecutive recapture of rigid nanoparticles using a solid-state nanopore sensor

Electrophoresis, 2018, 39(5-6), 833-843